Computational Energy Science

Vol. 2, No. 3, p. 55-62, 2025

Original article

Molecular dynamics study of H_2-oil mixture behavior in shale nanopores

Qiuhao Chang[1]*, Yuting Wu[2], Zhongyun Tian[3,4]

[1]*Department of Civil and Environmental Engineering, University of Canterbury, Christchurch 8041, New Zealand*
[2]*Department of Electrical and Computer Engineering, University of Wisconsin-Madison, WI 53706, United States*
[3]*School of Architecture and Design, Harbin Institute of Technology, Harbin 150001, P. R. China*
[4]*A IEIT SYSTEMS CO., LTD., Shandong 250101, P. R. China*

Keywords:
Underground hydrogen storage
residual pore oil
H_2 self-diffusion
molecular dynamics simulation

Cited as:
Chang, Q., Wu, Y., Tian, Z. Molecular dynamics study of H_2-oil mixture behavior in shale nanopores. Computational Energy Science, 2025, 2(3): 55-62.
https://doi.org/10.46690/compes.2025.03.01

Abstract:
With growing hydrogen demand and production, large-scale H_2 storage technologies are becoming increasingly essential. Depleted shale reservoirs, with their extensive pore space and existing subsurface infrastructure, offer a promising option for large-scale H_2 storage. In this study, the behavior of H_2 in shale nanopores in the presence of residual oil, which has not been well explored, is systematically investigated. It is observed that at 353 K and 30 MPa, residual oil weakens but does not completely prevent H_2 accumulation on pore surfaces, which may contribute to H_2 loss. Furthermore, decreasing pore size enhances H_2 surface accumulation due to nano-confinement effect, while increased oil saturation and smaller apertures reduce H_2 self-diffusion by restricting transport pathways. In addition, the phase of oil also plays a key role: supercritical methane mixes readily with H_2, whereas liquid n-butane, n-octane, and n-dodecane form clusters or oil bridges, further limiting H_2 mobility in nanopores. These findings provide molecular-scale insights into H_2-oil interactions and highlight the combined effects of residual oil saturation, pore size, and oil composition on H_2 retention and transport, which are critical for assessing the feasibility of underground H_2 storage in depleted shale reservoirs.

1. Introduction

Hydrogen, known for its potential as a clean energy carrier, is poised to play a pivotal role in the global transition toward net-zero emissions (Kovač et al., 2021). With applications spanning transportation, industrial feedstocks, and electricity generation, hydrogen demand is expected to rise significantly in the coming decades (Qazi, 2022). In 2020, global hydrogen production was approximately 90 million metric tons (Mt) and is projected to increase steadily. According to the Hydrogen Council, achieving carbon neutrality by 2050 will necessitate an estimated 660 Mt of hydrogen, representing approximately 22% of the total global energy demand. However, a critical barrier to such large-scale hydrogen utilization is the availability of efficient and cost-effective storage solutions. Conventional surface storage technologies, such as cryogenic tanks and high-pressure vessels, are limited by capacity constraints and high capital costs (Xie et al., 2024). Underground hydrogen storage (UHS) in porous media presents a viable alternative to overcome these storage challenges, facilitating the integration of hydrogen into the global energy landscape (Tarkowski, 2019; Zivar et al., 2021; Feng et al., 2024; Zhang et al., 2024).

Among various subsurface porous media, such as salt caverns and deep aquifers, depleted oil reservoirs offer significant advantages for underground hydrogen storage (UHS), including well-characterized geological structures, verified caprock integrity, and pre-existing infrastructure, all of which enhance their suitability for underground hydrogen storage (Sekar et al., 2023). For example, a field trial presented by Hellerschmied et al. (2024) reported an 84.3% hydrogen recovery for 119,353 m^3 of H_2 admixed with CH_4 in a depleted oil

Yandy Scientific Press

*Corresponding author.
E-mail address: qiuhao.chang@canterbury.ac.nz (Q. Chang); ywu0227@gmail.com (Y. Wu); zhongyun_tian@163.com (Z. Tian).

Received July 3, 2025; revised July 30, 2025; accepted August 31, 2025; available online September 5, 2025.

reservoir after 285 days of storage. Kanaani et al. (2022) suggested that hydrogen recovery during UHS in a depleted oil reservoir could reach 89.7% if CH_4 was used as the cushion gas according to their reservoir simulations. Lysyy et al. (2021) performed numerical simulations to investigate the storage of H_2 with CH_4 cushion gas in the mid-oil zone of the Norne field in Norway. The final hydrogen recovery in the oil zone reached 77% after 5 years. These high H_2 recovery efficiencies highlight the strong potential of depleted oil reservoirs for hydrogen storage.

The rapid expansion of global shale gas and oil production over the past two decades has resulted in a large number of depleted shale reservoirs. These formations present attractive candidates for UHS. H_2 recovery efficiency is largely determined by the flow dynamics and spatial distribution of H_2 within the nanopores of the shale formation. These behaviors are affected by the interactions between the injected gases and the residual pore fluids, including water and oil. For example, Mashhadzadeh and Faroughi (2025) reported that confinement effects reduce H_2 diffusion within slit nanopores, whereas higher temperatures weaken H_2-water interactions and consequently enhance its diffusivity. Wang et al. (2025) found that the presence of a water film along pore walls significantly suppresses H_2 diffusion, but high pressures within the nanopores can disrupt such film and promote bypass flow. Zhang et al. (2023) investigated H_2 dissolution in water-saturated kaolinite nanopores, revealing that nanoconfinement could enhance H_2 solubility by up to 27 times in a 0.55 nm slit pore. Bechara et al. (2022) studied the impact of H_2 on shale rocks and fluid properties to assess its potential for storage in depleted shale formations. Their results showed that H_2 not only altered the wettability of shale but also affected the viscosity of both crude oil and produced water. A study by Chen et al. (2024) indicates that CH_4 is preferentially adsorbed over H_2 in a CH_4/H_2 mixture, while H_2O molecules are preferentially adsorbed over both CH_4 and H_2 in a $CH_4/H_2/H_2O$ mixture. Such preferential adsorption of CH_4 and H_2O allows H_2 molecules to move freely in the nanopores, facilitating their recovery during the H_2 production process.

To date, researchers have mainly focused on H_2 behaviors such as adsorption, diffusion, and dissolution in the presence of pore water; however, the influence of residual oil on these H_2 properties remains poorly understood. Thus, this study, for the first time, investigates how the presence of crude oil affects H_2 self-diffusion and spatial distribution within shale nanopores of varying sizes under a geological condition of 353 K and 30 MPa. The manuscript is organized as follows: Section 2 presents the methodology and details of the MD simulation. Section 3 begins with validation cases for the MD simulations, followed by an analysis and discussion of the behavior of the H_2-oil system in shale nanopores. Finally, Section 4 summarizes the conclusions and outlines future work.

2. Models and simulation details

In this study, molecular dynamics (MD) simulations were employed to investigate H_2 behavior within nanopores in the presence of residual oil. MD simulation is a powerful computational method grounded in statistical mechanics and thermodynamics. By applying Newton's laws of motion, MD tracks particle positions, velocities, and interaction forces over time, generating a trajectory that captures the system's molecular evolution. This trajectory enables detailed analysis of both static and dynamic properties, as well as the calculation of various macroscopic physical parameters. MD is especially valuable for conditions that are difficult or impossible to reproduce experimentally, such as extreme pressures and temperatures (Jin et al., 2021), nanoscale confinement (Liu et al., 2022, 2023, 2023a, 2024; Shi et al., 2025), interfacial phenomena (Chang et al., 2024, 2024a; Yang et al., 2017, 2025), and complex molecular interactions (Kollman and Merz Jr, 1990; Tuckerman and Martyna, 2000; Chang et al., 2023).

We used the Large-scale Atomic/Molecular Massively Parallel Simulator (LAMMPS) for all MD simulations (Thompson et al., 2022). Quartz (α-SiO_2) is one of the most common minerals in shale formations (Shaw and Weaver, 1965), thus it was used to build the shale nanopores. A unit cell of α-SiO_2 was obtained from the Materials Studio database and was cleaved along the [0, 0, 1] direction. Subsequently, it was replicated (supercell) in the x, y, and z directions to form a two-layer pore wall with dimensions of 98.2 Å × 49.1 Å × 10.8 Å. By specifying a pore size (aperture) between the two pore walls, a slit nanopore model was developed. Four pore sizes including 2, 4, 6, and 8 nm were considered in this study. Moreover, to evaluate the impact of residual oil on gas behavior, varying amounts of crude oil (expressed as oil saturation, S_o) were introduced into the nanopores along with H_2. Different oil components, including n-methane (C_1), n-butane (C_4), n-octane (C_8), and n-dodecane (C_{12}), were separately incorporated as representative crude oil components to study how different hydrocarbons influence H_2 behaviors within the nanopores.

In the simulations, H_2 and oil molecules were randomly placed in the nanopore space at the initial condition. A 10 ns NVT run with a 1 fs time step was then performed to allow each system to reach equilibrium, with the temperature controlled using a Nosé-Hoover thermostat. During all simulations, the quartz surfaces were kept fixed, remaining stationary and rigid. The classical TraPPE force field with a united-atom (UA) style was used to model the interactions of the oil molecules. H_2 molecules were modelled using a validated single-site force field (Köster et al., 2018), while the SiO_2 layers were described using force fields developed by Cui et al. (2021) and Yu et al. (2023). These force fields have been validated for their reliability in simulating the related materials (Mosher et al., 2013; Xiong et al., 2017; Van Rooijen et al., 2023; Chang et al., 2023, 2026). The self-diffusion coefficient of the H_2 was calculated using the mean square displacement (MSD). MSD quantifies the average squared deviation of a particle's position from its initial location over time and is defined as (Yang et al., 2020):

$$MSD(t) = \left\langle |r_i(t) - r_i(0)|^2 \right\rangle \quad (1)$$

where $r_i(t)$ is the position of particle i at time t, and the angular

brackets denote an ensemble average. The self-diffusion coefficient (D) in a three-dimensional scale can then be obtained from the MSD via:

$$D = \lim_{t\to\infty} \frac{1}{6t} MSD(t) \quad (2)$$

3. Results and discussions

Validation of the molecular model and force field parameters is crucial for reliable MD simulation analysis. Density is an important property for validating force fields. Therefore, densities of H_2, C_1, and C_8 (representing long-chain n-alkanes) at 353 K and 30 MPa were determined and compared with values from the NIST database. As listed in Table 1, densities determined from our MD simulations agree well with the reference data.

Table 1. Density validation between MD simulation results and reference data.

	MD	NIST (g/cm^3)
H_2	0.0177	0.0177
C_1	0.163	0.167
C_8	0.684	0.686

In addition, we determined the density distribution profile of pure C_8 in a 5 nm quartz nanopore at 353 K and 30 MPa, as shown in Fig. 1. The obtained profile is consistent with the results reported by Wang et al. (2016), validating the force field used to simulate the interaction between the quartz nanopore and long-chain n-alkanes. Moreover, we specially constructed an H_2/C_1 mixture system (1:1 mole ratio) in a 5 nm quartz nanopore at approximately 343 K and 15 MPa, and determined the H_2/C_1 density profiles separately, as shown in Fig. 2. The density profiles of H_2 and C_1 are in good agreement with the results reported by Chen et al. (2024) under similar pressure and temperature conditions, further validating the force fields used to simulate the interactions between H_2, C_1 and the shale nanopore.

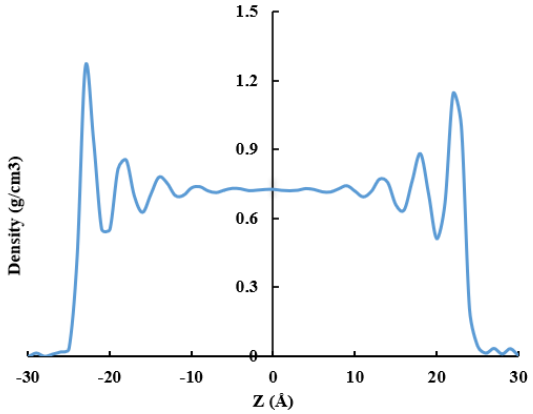

Fig. 1. Density profile of C_8 in the 5 nm slit pore at 353 K and 30 MPa.

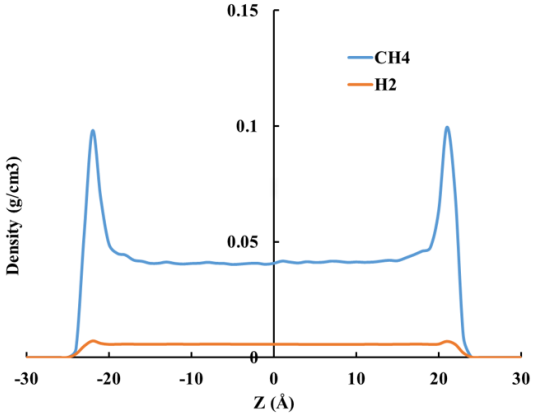

Fig. 2. Density profiles of C_8/C_1 gas mixture in a 5 nm slit pore at 343 K and 15 MPa.

To study the behavior of the H_2-oil system in nanopores, we first visualize the configuration of the H_2-C_8 system in a 4 nm slit pore with different oil saturations as an example, as shown in Fig. 3. In addition, the corresponding density profiles of C_8 and H_2 across the nanopore were determined and presented in Figs. 4 and 5. At a low oil saturation of 0.2, Fig. 3 shows that oil molecules tend to aggregate into clusters and accumulate on the pore surface, while H_2 molecules mainly reside in the center of the pore space, which is consistent with their density distribution profiles. As oil saturation increases, the oil phase expands and reduces the space available for H_2 molecules to move. At an oil saturation of 0.6, a small amount of H_2 molecules forms a gas bubble. At the highest oil saturation of 0.8, the gas phase no longer exists. Instead, H_2 molecules dissolve into the oil phase, and some accumulate on the pore surface. Unlike residual pore water, which can effectively inhibit H_2 accumulation on the quartz surface (Chen et al., 2024), H_2 accumulation on the quartz surface is observed at all oil saturation levels, although it is weakened by the presence of oil. This behavior may lead to H_2 loss during hydrogen storage in depleted shale reservoirs.

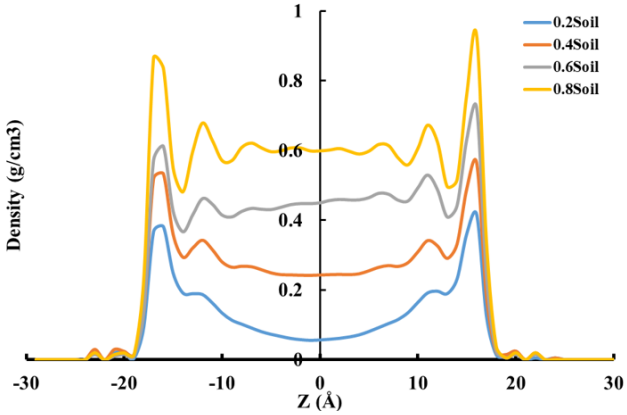

Fig. 4. Density profiles of C_8 in the H_2-C_8 system within a 4 nm nano pore at different oil saturations.

To investigate the impact of pore aperture on the behavior of H_2 and oil in quartz nanopores, the configuration of the H_2-C_8 system with 0.2 oil saturation in nanopores with different

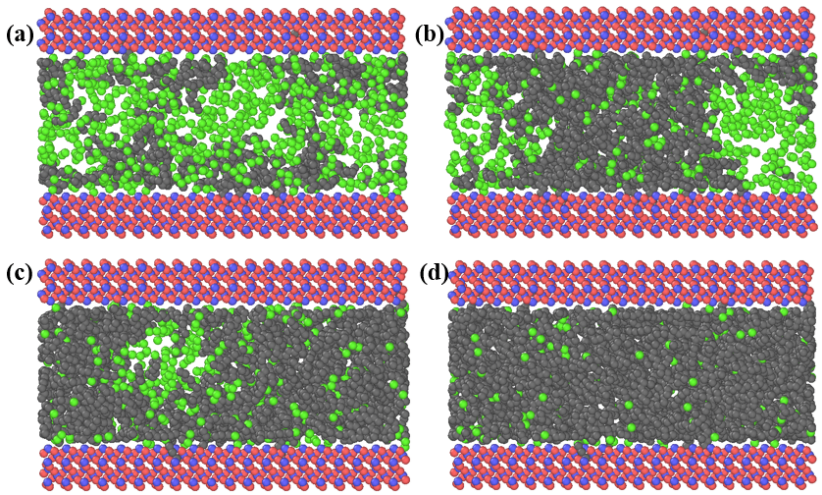

Fig. 3. Configurations of the H_2-C_8 system in a 4 nm slit pore with different oil saturations, (a) 0.2 Soil, (b) 0.4 Soil, (c) 0.6 Soil, and (d) 0.8 Soil. Black: C8 molecules, green: H_2.

apertures is visualized in Fig. 6 as a representative example. In addition, the relative density ratio, defined as the local density in the nanopores divided by the bulk density, was determined in Figs. 7 and 8 to illustrate the preferential distribution of H_2 and oil in nanopores with different apertures. According to the configurations and density profiles, it is clear that oil molecules mainly distribute near the pore surface. However, as the pore aperture decreases, the oil relative density ratio in the middle region increases, indicating that oil molecules move more easily into the central region of the nanopore with smaller apertures. In addition, the relative density ratio of H_2 near the pore surface increases as the pore aperture decreases, indicating that the nano-confinement effect enhances the accumulation of H_2 on the pore surface even in the presence of residual oil.

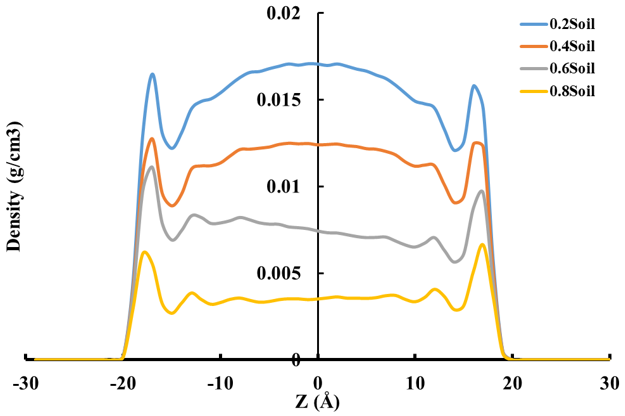

Fig. 5. Density profiles of H_2 in the H_2-C_8 system within a 4 nm nano pore at different oil saturations.

The self-diffusion coefficients of H_2 in the H_2-C_8 system with varying oil saturations in nanopores with different apertures are shown in Fig. 9. As oil saturation increases, more oil molecules occupy the pore space, constricting the movement of H_2 molecules and leading to a consistent decrease in H_2 self-diffusion. Moreover, as the pore aperture decreases, we believe there are two reasons that contribute to the decrease in H_2 self-diffusion coefficients. First, the nano-confinement effect is enhanced as the aperture decreases, slowing down gas self-diffusion (Spera and Franco, 2020; Lyu et al., 2022). Second, in smaller nanopores, oil molecules can more easily move toward the center of the pore compared to larger nanopores, which may also restrict H_2 self-diffusion within the nanopores.

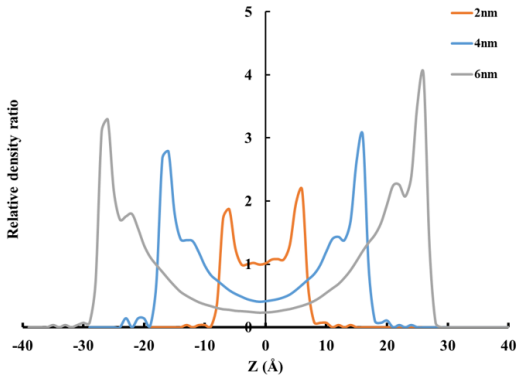

Fig. 7. Relative density ratio of C_8 in the H_2-C_8 system with 0.2 oil saturation in nanopores with different sizes.

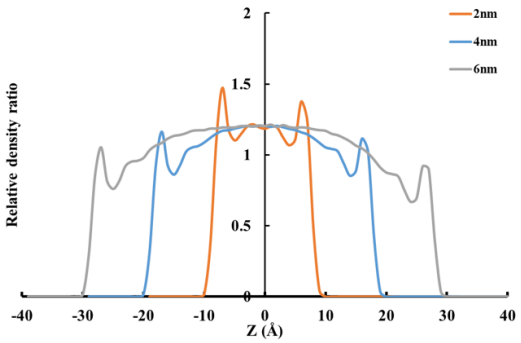

Fig. 8. Relative density ratio of H_2 in the H_2-C_8 system with 0.2 oil saturation in nanopores with different sizes.

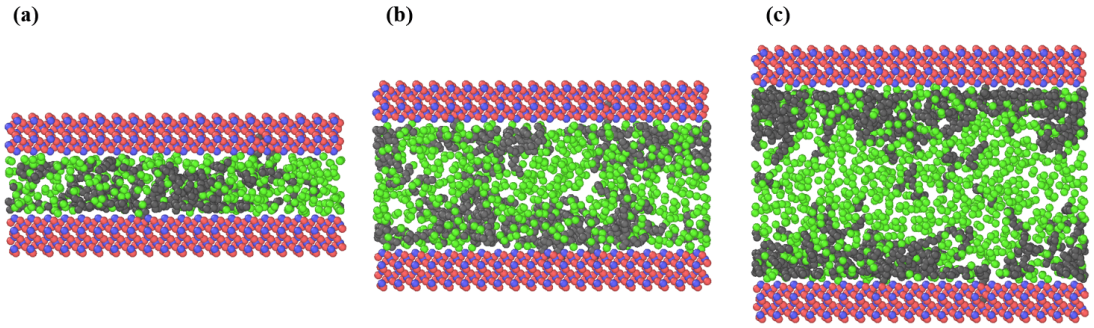

Fig. 6. Configurations of H_2-C_8 system with 0.2 oil saturation in nanopores with (a) 2 nm aperture, (b) 4 nm aperture, and (c) 6 nm aperture.

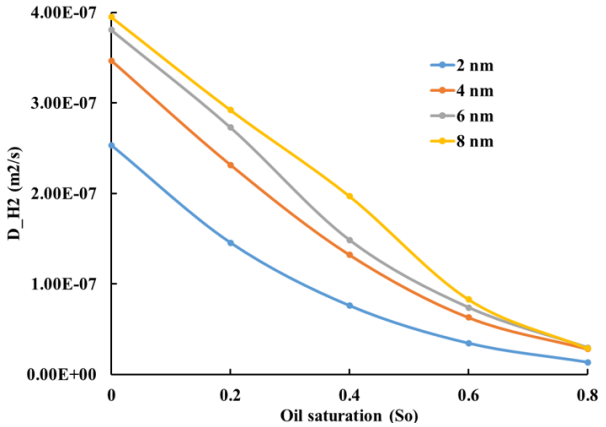

Fig. 9. Self-diffusion coefficients of H_2 in the H_2-C_8 system within nanopores with different pore sizes.

In addition to C_8, the behavior of H_2 in interactions with other common oil components within quartz nanopores was also investigated, including C_1, C_4, and C_{12}. As an example, at an oil saturation of 0.2, the configurations of H_2 with C_1-C_{12} separately in a 4 nm nanopore are shown in Fig. 10, and the corresponding density profiles of oil and H_2 are depicted in Figs. 11 and 12 respectively. At 353 K and 30 MPa, C_1 exists in a supercritical state, whereas C_4, C_8, and C_{12} are in the liquid phase. Consequently, as shown in Fig. 10(a), C_1 readily mixes with H_2, and the densities of H_2 and C_1 are relatively uniformly distributed along the nanopore, with pronounced accumulation near the pore surface. In contrast, the liquid components C_4, C_8, and C_{12} mix less readily with gaseous H_2, leading to the formation of oil clusters (Figs. 10(b) and 10(c)) and oil-bridging (Fig. 10(d)) structures within the nanopore. Correspondingly, oil clusters of C_4 and C_8 on the pore surface result in high oil densities near the pore wall, whereas the formation of an oil bridge by C_{12} leads to higher oil densities in the central region of the nanopore compared to the clustered cases.

Fig. 13 shows the H_2 self-diffusion coefficients within a 4 nm nanopore in the presence of different oils. For the H_2-C_1 system, since C_1 has a larger molecular weight than H_2 and diffuses more slowly than H_2, its interaction with H_2 leads to a reduction in the self-diffusion coefficient of H_2. In addition, as the amount of C_1 present in the nanopore increases, the interaction between H_2 and C_1 is further enhanced, resulting in an additional decrease in H_2 self-diffusion. A significant reduction in H_2 self-diffusion is observed when H_2 coexists with C_4, C_8, and C_{12}. This is likely because these oil components with larger MW are in the liquid state under simulated conditions and do not mix with H_2 as readily as C_1, occupying the pore volume and restricting the space available for H_2 transport, thereby markedly reducing H_2 self-diffusion.

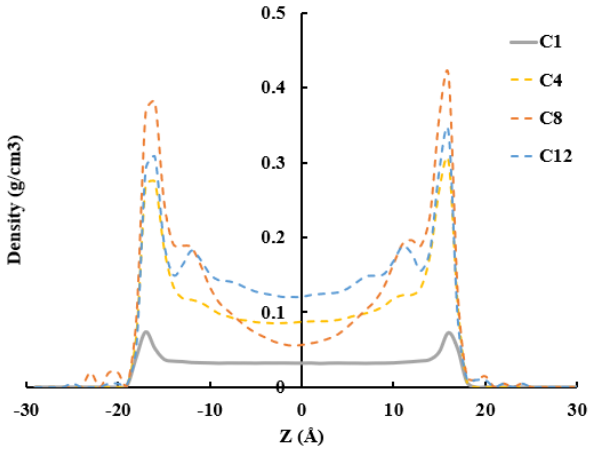

Fig. 11. Oil density profiles in a 4 nm nanopore at 0.2 oil saturation for C_1-C_{12} separately.

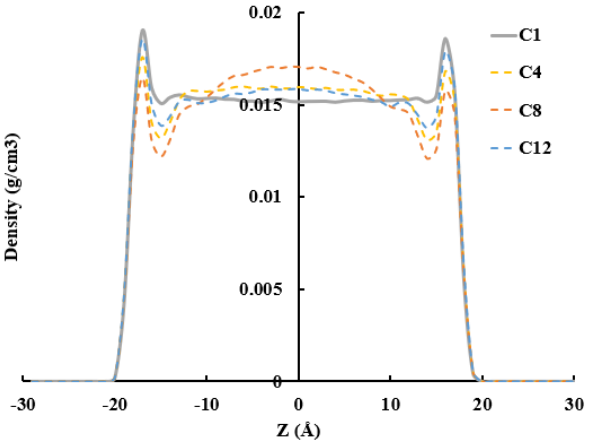

Fig. 12. H_2 density profiles in a 4 nm nanopore at 0.2 oil saturation with C_1-C_{12} separately.

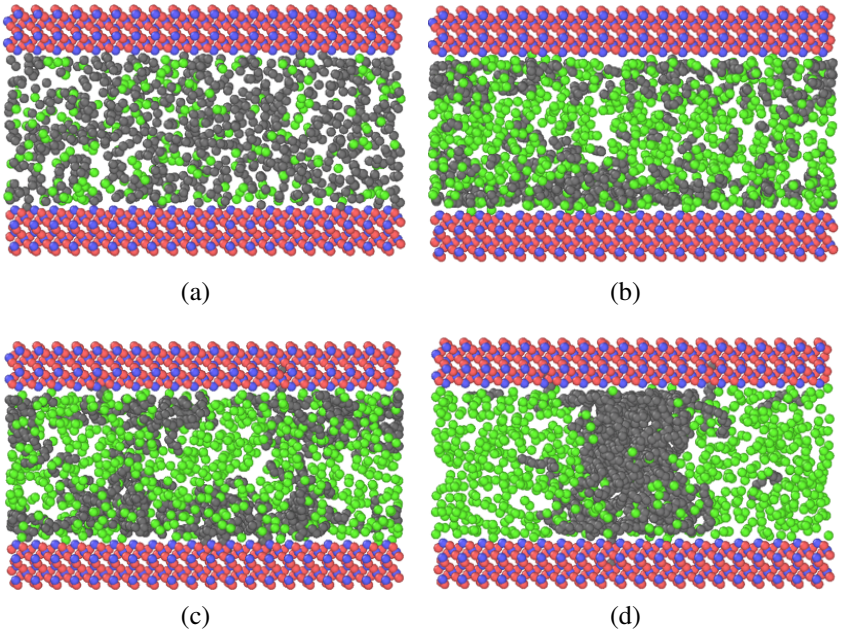

Fig. 10. Configurations of the H_2-oil system at an oil saturation of 0.2 in a 4 nm nanopore for (a) C_1, (b) C_4, (c) C_8 and (d) C_{12}.

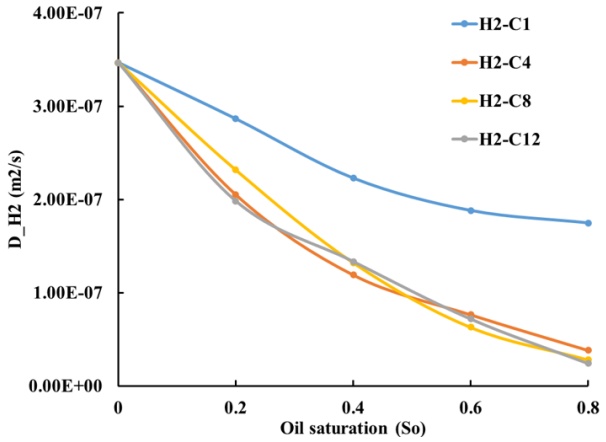

Fig. 13. Self-diffusion coefficients of H_2 in a 4 nm nanopore with different n-alkanes.

4. Conclusions and outlook

In this study, molecular dynamics simulations were employed to systematically investigate the behavior of H_2 in shale nanopores in the presence of residual oil, with particular emphasis on the effects of oil saturation, pore aperture, and oil composition. The results demonstrate that residual oil cannot completely inhibit H_2 accumulation on the pore surface. H_2 accumulation is observed at all oil saturation levels, although it is weakened by the presence of oil, suggesting a potential mechanism for H_2 loss during underground hydrogen storage (UHS) in depleted shale reservoirs. Oil molecules preferentially adsorb near the pore surface, while decreasing pore aperture promotes oil migration toward the central region of the nanopore. Simultaneously, as pore size decreases, the nano-confinement effect enhances H_2 surface accumulation even in the presence of residual oil. These confinement effects, together with increasing oil saturation, significantly reduce H_2 self-diffusion by constricting its transport pathway. Furthermore, the impact of oil composition on H_2 behavior is found to be strongly phase dependent. Supercritical C_1 readily mixes with H_2, resulting in relatively uniform density distributions, whereas liquid C_4, C_8, and C_{12} exhibit poor miscibility with H_2 and form oil clusters or oil-bridging structures that significantly restrict H_2 mobility. Based on this study, future work should focus on experimental validation of these simulation results and extend to the investigation of key factors relevant to UHS. In particular, the effects of cushion gases (e.g., CO_2 and N_2) and geological conditions, such as pressure, temperature, and salinity, on H_2-oil behavior and n-alkane phase states should be systematically examined. Such studies will further strengthen understanding and provide a solid basis for the design of efficient underground hydrogen storage strategies in depleted shale reservoirs.

Conflict of interest

The authors declare no competing interest.

References

Bechara, E., Gamadi, T., Hussain, A., et al. Effect of hydrogen exposure on shale reservoir properties and evaluation of hydrogen storage possibility in depleted unconventional formations. Unconventional Resources Technology Con-

ference (URTeC), 2022: 1734-1748.

Chen, F., Wang, S., Dejam, M., et al. Molecular simulation of competitive adsorption of hydrogen and methane: analysis of hydrogen storage feasibility in depleted shale gas reservoirs. SPE Journal, 2024, 29(6): 3412-3422.

Chang, Q., Huang, L., McKenzie, K., et al. Influence of hydrogen sulfide on gas-water interface in underground hydrogen storage: A molecular dynamics study. Journal of Energy Storage, 2024, 97: 112766.

Chang, Q., Dempsey, D., Zhang, L., et al. Molecular dynamics insights into gas-water interfacial tension: Optimizing hydrogen storage in subsurface conditions. International Journal of Hydrogen Energy, 2024a, 64: 896-905.

Chang, Q., Edgar III, A. O., Ghos, S., et al. An atomistic model of aged asphalt guided by the oxidation chemistry of benzylic carbon with application to asphalt rejuvenated with a triglyceride. Construction and Building Materials, 2023, 400: 132743.

Cui, S., Fu, J., Guo, M., et al. Diffusion of high-temperature and high-pressure CH_4 gas in SiO_2 nanochannels. Frontiers in Energy Research, 2021, 9: 667640.

Chang, Q., Huang, L., Wu, X. A molecular dynamics study on low-pressure carbon dioxide in the water/oil interface for enhanced oil recovery. SPE Journal, 2023, 28(2): 643-652.

Chang, Q., Dempsey, D., Huang, L. Determination of interfacial tension for H_2-H_2S-water and CH_4-H_2S-water mixtures under different geological conditions for underground hydrogen storage. Journal of Energy Storage, 2026, 143: 119683.

Feng, X., Liu, J., Shi, J., et al. Phase equilibrium, thermodynamics, hydrogen-induced effects and the interplay mechanisms in underground hydrogen storage. Computational Energy Science, 2024, 1(1): 46-64.

Hellerschmied, C., Schritter, J., Waldmann, N., et al. Hydrogen storage and geo-methanation in a depleted underground hydrocarbon reservoir. Nature Energy, 2024, 9(3): 333-344.

Jin, L., He, Y., Zhou, G., et al. Natural gas density under extremely high pressure and high temperature: Comparison of molecular dynamics simulation with corresponding state model. Chinese Journal of Chemical Engineering, 2021, 31: 2-9.

Kovač, A., Paranos, M., Marciuš, D. Hydrogen in energy transition: A review. International Journal of Hydrogen Energy, 2021, 46(16): 10016-10035.

Kanaani, M., Sedaee, B., Asadian-Pakfar, M. Role of cushion gas on underground hydrogen storage in depleted oil reservoirs. Journal of Energy Storage, 2022, 45: 103783.

Kollman, P. A., Merz Jr, K. M. Computer modeling of the interactions of complex molecules. Accounts of Chemical Research, 1990, 23(8): 246-252.

Köster, A., Thol, M., Vrabec, J. Molecular models for the hydrogen age: Hydrogen, nitrogen, oxygen, argon, and water. Journal of Chemical & Engineering Data, 2018, 63(2): 305-320.

Lysyy, M., Fernø, M., Ersland, G. Seasonal hydrogen storage in a depleted oil and gas field. International Journal of Hydrogen Energy, 2021, 46(49): 25160-25174.

Liu, J., Zhang, T., Sun, S. Mechanism analysis of shale gas adsorption under carbon dioxide-moisture conditions: A molecular dynamic study. Energy & Fuels, 2022, 36(24): 14865-14873.

Liu, J., Zhang, T., Sun, S. Absorption of carbon dioxide in kerogen nanopores: A mechanism study using the molecular dynamics Monte Carlo method. arxiv preprint arxiv: 2308.05116, 2023.

Liu, J., Zhang, T., Sun, S. Molecular dynamics simulations of ion transport through protein nanochannels in peritoneal dialysis. International Journal of Molecular Sciences, 2023a, 24(12): 10074.

Liu, J., Zhang, T., Sun, S. Molecular insights into the carbon dioxide sequestration in kerogen: An accelerated algorithm coupling molecular dynamics simulations and Monte Carlo methods. Process Safety and Environmental Protection, 2024, 185: 1336-1351.

Lyu, F., Ning, Z., Yang, S., et al. Molecular insights into supercritical methane sorption and self-diffusion in monospecific and composite nanopores of deep shale. Journal of Molecular Liquids, 2022, 359: 119263.

Mashhadzadeh, A. H., Faroughi, S. A. Atomistic simulation of dilute hydrogen in water-saturated kaolinite nanopores: Implications for underground hydrogen storage. International Journal of Hydrogen Energy, 2025, 109: 1358-1371.

Mosher, K., He, J., Liu, Y., et al. Molecular simulation of methane adsorption in micro-and mesoporous carbons with applications to coal and gas shale systems. International Journal of Coal Geology, 2013, 109: 36-44.

Qazi, U. Y. Future of hydrogen as an alternative fuel for next-generation industrial applications; challenges and expected opportunities. Energies, 2022, 15(13): 4741.

Sekar, L. K., Kiran, R., Okoroafor, E. R., et al. Review of reservoir challenges associated with subsurface hydrogen storage and recovery in depleted oil and gas reservoirs. Journal of Energy Storage, 2023, 72: 108605.

Shi, J., Zhang, T., Sun, S., et al. Ab Initio Insights into the CO_2 Adsorption Mechanisms in Hydrated Silica Nanopores. Chemical Engineering Science, 2025: 121741.

Shaw, D. B., Weaver, C. E. The mineralogical composition of shales. Journal of Sedimentary Research, 1965, 35(1): 213-222.

Spera, M. B., Franco, L. F. Surface and confinement effects on the self-diffusion coefficients for methane-ethane mixtures within calcite nanopores. Fluid phase equilibria, 2020, 522: 112740.

Tarkowski, R. Underground hydrogen storage: Characteristics and prospects. Renewable and Sustainable Energy Reviews, 2019, 105: 86-94.

Tuckerman, M. E., Martyna, G. J. Understanding modern molecular dynamics: Techniques and applications. The Journal of Physical Chemistry B, 2000, 104(2): 159-178.

Thompson, A. P., Aktulga, H. M., Berger, R., et al. LAMMPS-a flexible simulation tool for particle-based materials modeling at the atomic, meso, and continuum scales. Computer physics communications, 2022, 271: 108171.

Tarkowski, R. Underground hydrogen storage: Characteristics and prospects. Renewable and Sustainable Energy Reviews, 2019, 105: 86-94.

Tuckerman, M. E., Martyna, G. J. Understanding modern molecular dynamics: Techniques and applications. The Journal of Physical Chemistry B, 2000, 104(2): 159-178.

Thompson, A. P., Aktulga, H. M., Berger, R., et al. LAMMPS-a flexible simulation tool for particle-based materials modeling at the atomic, meso, and continuum scales. Computer physics communications, 2022, 271: 108171.

Van Rooijen, W. A., Habibi, P., Xu, K., et al. Interfacial tensions, solubilities, and transport properties of the $H_2/H_2O/NaCl$ system: A molecular simulation study. Journal of Chemical & Engineering Data, 2023, 69(2): 307-319.

Wang, K., Han, R., Sun, Q. Molecular Dynamics Study of the H_2-CO_2-H_2O Mixture Flow Through Silica Nanopores. SPE Journal, 2025, 30(10): 6496-6510.

Wang, S., Javadpour, F., Feng, Q. Molecular dynamics simulations of oil transport through inorganic nanopores in shale. Fuel, 2016, 171: 74-86.

Xie, Z., Jin, Q., Su, G., et al. A review of hydrogen storage and transportation: Progresses and challenges. Energies, 2024, 17(16): 4070.

Xiong, J., Liu, X., Liang, L., et al. Adsorption of methane in organic-rich shale nanopores: An experimental and molecular simulation study. Fuel. 2017, 200: 299-315.

Yang, Y., Narayanan Nair, A. K., Sun, S. Molecular dynamics simulation study of carbon dioxide, methane, and their mixture in the presence of brine. The Journal of Physical Chemistry B, 2017, 121(41): 9688-9698.

Yang, Y., Nair, A. K. N., Sun, S., et al. Estimating fluid-solid interfacial free energies for wettabilities: A review of molecular simulation methods. Advances in Colloid and Interface Science, 2025: 103482.

Yu, T., Li, Q., Tan, Y., et al. Effect mechanism of wettability on CO_2 replacement brine in nanopores. Journal of Hydrology, 2023, 625: 130165.

Yang, Y., Narayanan Nair, A. K., Sun, S. Orption and diffusion of methane and carbon dioxide in amorphous poly (alkyl acrylates): A molecular simulation study. The Journal of Physical Chemistry B, 2020, 124(7): 1301-1310.

Zivar, D., Kumar, S., Foroozesh, J. Underground hydrogen storage: A comprehensive review. International journal of hydrogen energy, 2021, 46(45): 23436-23462.

Zhang, T., Liu, J., Yang, X., et al. Advances in the microscopic and mesoscopic simulation technologies developed for subsurface gas storage. Advances in Geo-Energy Research, 2024, 14(1): 1-3.

Zhang, H., Luo, X., Yang, D., et al. Molecular simulation of H_2 loss by dissolution in caprock water-saturated nanopores under the nanoconfinement effect for underground hydrogen storage. Energy & Fuels, 2023, 37(23): 19357-19368.